Journal of Power Sources 191 (2009) 320–329

Contents lists available at ScienceDirect

Journal of Power Sources

journal homepage: www.elsevier.com/locate/jpowsour

Characterization of metal-supported axial injection plasma sprayed solid oxide fuel cells with aqueous suspension plasma sprayed electrolyte layers

D. Waldbillig[a], O. Kesler[b,*]

[a] University of British Columbia, Department of Materials Engineering, 309-6350 Stores Road, Vancouver, BC, Canada V6T 1Z4
[b] University of Toronto, Department of Mechanical and Industrial Engineering, 5 King's College Road, Toronto, Ontario, Canada M5S 3G8

ARTICLE INFO

Article history:
Received 19 December 2008
Received in revised form 22 January 2009
Accepted 28 January 2009
Available online 7 February 2009

Keywords:
Solid oxide fuel cell
Plasma spraying
Suspension
Yttria stabilized zirconia
Electrolyte
Metal support

ABSTRACT

A method for manufacturing metal-supported SOFCs with atmospheric plasma spraying (APS) is presented, making use of aqueous suspension feedstock for the electrolyte layer and dry powder feedstock for the anode and cathode layers. The cathode layer was deposited first directly onto a metal support, in order to minimize contact resistance, and to allow the introduction of added porosity. The electrolyte layers produced by suspension plasma spraying (SPS) were characterized in terms of thickness, permeability, and microstructure, and the impact of substrate morphology on electrolyte properties was investigated. Fuel cells produced by APS were electrochemically tested at temperatures ranging from 650 to 750 °C. The substrate morphology had little effect on open circuit voltage, but substrates with finer porosity resulted in lower kinetic losses in the fuel cell polarization.

1. Introduction

The demand for energy continues to increase and with it, interest has grown in alternatives to hydrocarbon fuels and increased energy efficiency. Fuel cells have been proposed as energy conversion devices that have the potential to address both of these issues [1].

Fuel cells electrochemically oxidize fuel to directly produce electricity and heat. There are a number of different types of fuel cells currently being developed, but one of the most promising is the solid oxide fuel cell (SOFC). This fuel cell type uses an ionically conductive ceramic material (often yttria stabilized zirconia—YSZ) as the electrolyte. Because ceramic materials typically have low and thermally activated electrical conductivities and high stability at elevated temperatures, SOFCs typically operate at temperatures between 600 and 1000 °C. Elevated temperature operation helps to reduce electrochemical losses and facilitates the use of high quality waste heat in cogeneration applications. The high operating temperature and oxide ion conducting nature of SOFCs also gives them the ability to use a wide variety of fuels such as hydrogen, natural gas, alcohols, and liquid hydrocarbons.

SOFCs are typically manufactured using wet ceramic techniques such as tape casting and screen printing or aerosol spraying combined with multiple high temperature (up to 1400 °C) sintering steps [2]. This makes large scale manufacturing based on these processes capital-intensive and time-consuming for mass production, and makes the use of low-cost metallic supports challenging.

Recently, it has been proposed to replace the current state-of-the-art Ni–YSZ cermet substrates with porous stainless steel substrates [3]. These metallic substrates have superior thermal, mechanical, and electrical properties to the cermet ones and are less expensive. However, it is difficult to incorporate metallic substrates into current manufacturing processes due to the high sintering temperature required to fully densify electrolyte layers. Inert atmosphere sintering with electrolyte sintering aids has been used to address these issues; however, inert atmospheres increase process costs and sintering aids usually introduce some level of electronic conductivity into the electrolyte, which decreases cell performance [4]. Plasma spraying (PS) has been proposed as a novel manufacturing method for SOFCs to address these issues with conventional manufacturing methods [1,5,6].

Plasma spraying is a well-established manufacturing technique first developed in the 1960s to produce value added coatings to enhance wear resistance, temperature resistance, and to repair parts [7]. Plasma sprayed coatings are most commonly used as thermal barrier coatings in gas turbines and diesel engines. Plasma spraying uses a hot, energetic plasma to melt feedstock powders, which impact with a substrate and rapidly solidify, forming solid splats. Subsequent splats form on previously deposited ones to produce coatings. Plasma temperatures may be up to 10,000 K, so in theory any material may be deposited. Fully sintered coatings may be produced rapidly without the need for post-deposition heat

* Corresponding author. Tel.: +1 416 978 3835; fax: +1 416 978 7753.
E-mail address: kesler@mie.utoronto.ca (O. Kesler).

0378-7753/$ – see front matter © 2009 Elsevier B.V. All rights reserved.
doi:10.1016/j.jpowsour.2009.01.084

treatments. This ability to rapidly produce ceramic layers without post-deposition sintering processes can allow metal-supported SOFCs to be manufactured rapidly and relatively inexpensively.

Most of the original plasma sprayed SOFC work used vacuum plasma spraying (VPS) techniques. The German aerospace center (DLR) has produced VPS SOFCs for many years [8–10]. VPS operates in low pressure atmospheres, which enable a longer and less turbulent plasma flame to be formed. Unfortunately, VPS systems require more equipment and are more expensive to operate [7] and thus much recent interest has arisen in developing methods to produce plasma sprayed SOFCs using atmospheric plasma spray (APS) systems that operate at atmospheric pressure [5].

Plasma spray systems usually use feedstock powders that are typically 10–100 μm in diameter. The powders are typically delivered by suspending them in a flowing gas, and most plasma spray SOFC research has focused on using these conventional powder spraying routes to produce fuel cell layers (e.g. [11,12]). However, it is challenging to produce fuel cell microstructures with the required properties, since it is difficult to feed powders <5 μm in diameter [1] and due to the horizontal splat orientation of the microstructure. It is also quite challenging to find spraying conditions to produce the porous, high surface area microstructures required for high performing SOFC composite electrodes or thin (<10 μm), fully dense microstructures required for electrolytes.

Recently, plasma spray systems have been modified in order to use nano- to micro-sized powders suspended in a liquid as feedstocks [13–18]. These smaller powders improve the ability of plasma spraying to produce finer microstructures and controlled porosity. However, much work remains to be done to develop methods to deliver and atomize the suspension, to deal with the liquid effects on the plasma, and to find optimal spraying conditions to produce layers with the desired microstructures.

Many suspension plasma spraying (SPS) SOFC studies have used relatively low powered plasma torches and have injected the feedstock suspensions radially. Low torch power limits the ability to use high solid content suspensions and often requires suspensions to be alcohol based [19] to lower the energy required to vapourize the suspending liquid. The low solid content limitations reduce coating deposition rates, and non-aqueous suspensions are typically more expensive and less environmentally friendly than water based ones. Radial injection of feedstock suspensions makes suspension atomization, droplet size, and velocity extremely important parameters, because it is very difficult to achieve good penetration of nano- to micro-sized suspended powders from the periphery to the center of the plasma plume. Axial injection of feedstock suspensions simplifies a number of injection issues, as the suspension is fed directly into the center of the plasma plume and thus does not have to pass through the more turbulent outer fringes of the plasma. However, axial feedstock injection increases the complexity of the plasma torch and limits the size of suspension feeding lines, since the lines have to pass between the torch electrodes.

Many previous studies have focused on spraying individual SOFC layers or on depositing layers on standard plasma spray substrates (sand blasted glass or steel plate). However, the substrate parameters can have a large effect on coating properties, and thus coatings sprayed on sand blasted flat sheet substrates may have very different properties to those of coatings sprayed on porous SOFC substrates. In addition, due to the multi-layer nature of SOFCs, it is very important to deposit each subsequent layer on top of a previously deposited fuel cell layer in order to better duplicate the substrate heat transfer conditions that would be observed during fuel cell manufacturing. Thus the deposition of anodes or cathodes directly onto porous metal substrates and of electrolyte layers onto previously sprayed anode or cathode layers allows the effect of surface morphology of substrates and initial coating on subsequent coatings to be determined.

This work reports initial results in the development of a fully plasma sprayed SOFC deposited on a porous stainless steel support. A high powered axial injection plasma spray torch was used to deposit cathode, electrolyte, and anode layers. Composite LSM/YSZ cathodes and NiO/YSZ anodes were deposited from conventional powder feedstocks. High solid content (23.7 wt%) aqueous YSZ suspensions were used as feedstocks for electrolyte layers. Full cells were built up by the sequential deposition of cathode, electrolyte and anode layers on the porous metallic substrate. This study focuses mainly on SPS electrolyte development and substrate selection, and selected electrolyte suspension plasma spray parameter optimization studies are reported. Cathode and anode spray parameters are being optimized in parallel studies and are reported elsewhere (e.g. [20]).

The cathode-first deposition configuration was selected due to the potential to obtain several benefits compared to the more traditional anode-first deposition configuration commonly used in the manufacture of planar cells. First, because the cathode is typically entirely made of hard ceramic, while the anode is traditionally a cermet composite with more compliant metal present, the anode can more readily establish a good electrical contact with the interconnect through mild deformation when loaded in a stack, so by spraying the cathode directly onto the metallic support, the melting of the cathode material and its solidification directly onto the metal, following the substrate contours, has the potential to establish a good electrical contact without the use of wet contact pastes. In addition, since metal has a higher thermal conductivity than the zirconia used in the electrolyte, the deposition of the cathode directly onto the metal has the potential to remove heat more rapidly than if the cathode were deposited onto a ceramic layer. This rapid heat removal provides a mechanism for the introduction of additional porosity into the cathode by allowing the more rapid freezing of partially melted structures to create porosity through partial melting, which is more critical for the cathode than for the anode, since the latter can obtain additional porosity through the reduction of NiO to Ni prior to operation of the cell.

Furthermore, the formation of a direct contact between the cathode and interconnect can reduce the extent of oxidation at the porous metal support–cathode interface, thus decreasing the extent of series resistance increase with time. Finally, the establishment of a pre-formed contact between cathode and metal support allows coatings for the minimization of oxidation and chromium evaporation to be placed on the metal after the electrical contact between the cathode and porous metal has been established. As a result, the protective coatings do not have to be electrically conductive, and so they can be designed to obtain the closest match in thermal expansion with the porous metal, or for ease of processing, without the additional requirement of electrical conductivity limiting the choice of materials.

Initially very energetic plasma spraying conditions were chosen in order to ensure full evaporation of the water and melting of the YSZ. After the initial spray runs, preheat temperature, standoff distance, and number of deposition passes were varied to determine their effect on electrolyte permeability and deposition efficiency to develop a more optimized process window.

The effect of two different porous stainless steel substrate types, denoted as media grades (MG) 2 and 5, were examined during this study. Both substrate types have comparable total porosity levels, but MG 5 has larger surface pores. These pores can enhance layer adhesion by facilitating the mechanical interlocking of the sprayed cathode with the rough substrate; however, some of the pores are too large for the splats to bridge over, which can result in discontinuous layers. The effect of substrate media grade on the surface roughness, permeability, and microstructure of deposited fuel cell layers is examined.

Table 1
Plasma spraying parameter values.

Parameter	Cathode	Electrolyte	Anode
Feedstock	48.2 wt% LSM/51.8 wt% YSZ powder	23.7 wt% YSZ aqueous suspension	46 wt% NiO/38 wt% YSZ/16 wt% carbon black powder
Particle size	−45 + 32 μm/−32 + 25 μm	D_{50} = 1.6 μm	−45 + 32 μm/D_{50} = 5.9 μm/10–30 μm
Plasma gas flow rate (slpm)	250	220	250
Plasma gas composition	23.3% N_2, 76.7% Ar	80% N_2, 20% H_2	23.3% N_2, 76.7% Ar
Torch current (A per cathode)	183	250	183
Nozzle size (mm)	9.5	12.7	12.7
Number of passes	60	25, **50**, 100[a]	80
Preheat temperature (°C)	300	20, **325**, 450[a]	300
Standoff distance (mm)	100	70, **80**, 90[a]	100

[a] Values in bold were held fixed during variation of other parameters.

Finally, full cells consisting of an APS cathode and anode and an SPS electrolyte on a porous metal support were fabricated and electrochemically tested.

2. Experimental procedure

2.1. Material preparation

A mixture of 48.2 wt% lanthanum strontium manganite (LSM) and 51.8 wt% 8 mol% yttria stabilized zirconia (YSZ) powders (Inframat Advanced Materials, Farmington, CT, USA) were used for the cathode layers. Spray dried cathode powders were sieved and mechanically mixed before plasma spraying. The detailed powder preparation procedure has been reported previously [20], and the powder size range is given in Table 1.

8 mol% (YSZ) powder (Inframat Advanced Materials, Farmington, CT, USA) was used as the electrolyte feedstock for this study. The as-received powder had a D_{50} agglomerate size of approximately 1.6 μm, with sizes ranging from 0.5 to 15 μm, as determined by laser light scattering (Mastersizer 2000, Malvern Instruments, Worcestershire, UK) (Fig. 1). Aqueous YSZ suspensions with a solid loading of 5 vol% (23.7 wt%) were prepared using deionized water. PBTCA (2-phosphonobutane-1,2,4-tricarboxylic acid) was used to enhance the particle dispersion in the suspensions. An optimized dispersant concentration was determined in a previous study [21].

Anode powders were sieved and then mechanically mixed. The powder consisted of a mixture of 46 wt% NiO (Novamet Specialty Products, Wyckoff, NJ, USA), 38 wt% YSZ (Inframat Advanced Materials, Farmington, CT, USA), and 16 wt% carbon black pore former (Osaka Gas Chemicals Co., Osaka, Japan). The anode powder size ranges are given in Table 1. The NiO powder size was controlled by sieving. The YSZ anode powder, whose particles all passed through the smallest sieve available (25 μm), was characterized by laser light scattering. The carbon powder passed through the smallest sieve and also could not be characterized with the available laser light scattering equipment due to the inability to disperse the carbon in an aqueous suspension. Therefore, the size range of the carbon powder was determined by scanning electron microscopy.

2.2. Plasma spray processing

An Axial III Series 600 (Northwest Mettech Corp., North Vancouver, BC, Canada) atmospheric plasma spray system was used for all layer depositions (Fig. 2a). This torch injects the feedstock axially between three electrodes, which ensures that virtually all of the powder injected passes through the hottest part of the plasma jet. For cathode and anode layers a Thermico (model CPF-2HP, Germany) powder feeding system was used. For the electrolyte layer, the plasma spraying system was modified to add a pressure vessel in order to deliver the suspension to the feed tube of the plasma torch (Fig. 2b). The suspension was injected through a needle type nozzle (ID = 0.84 mm) positioned directly behind the torch convergence into the centre of the plasma jet, where it was atomized.

The substrates were preheated directly by the plasma torch, before the powder or suspension feeding systems were turned on, to a temperature above the desired preheat temperature, and then were allowed to cool to the desired preheat temperature while the powder/suspension flow stabilized. Substrate temperatures during spraying were measured directly by positioning a Type K thermocouple in contact with the back of the metal substrate, and were monitored during spraying. Fig. 3 shows the temperature profile measured during a typical spraying run.

Deposition was carried out onto 2.54 cm diameter porous 430 ferritic stainless steel substrates (Mott Corporation, Farmington, CT, USA) mounted on a rotating turntable. Two different media grades of stainless steel substrates were examined, MG 2 and MG 5. These substrates are most commonly used as filter media, and the

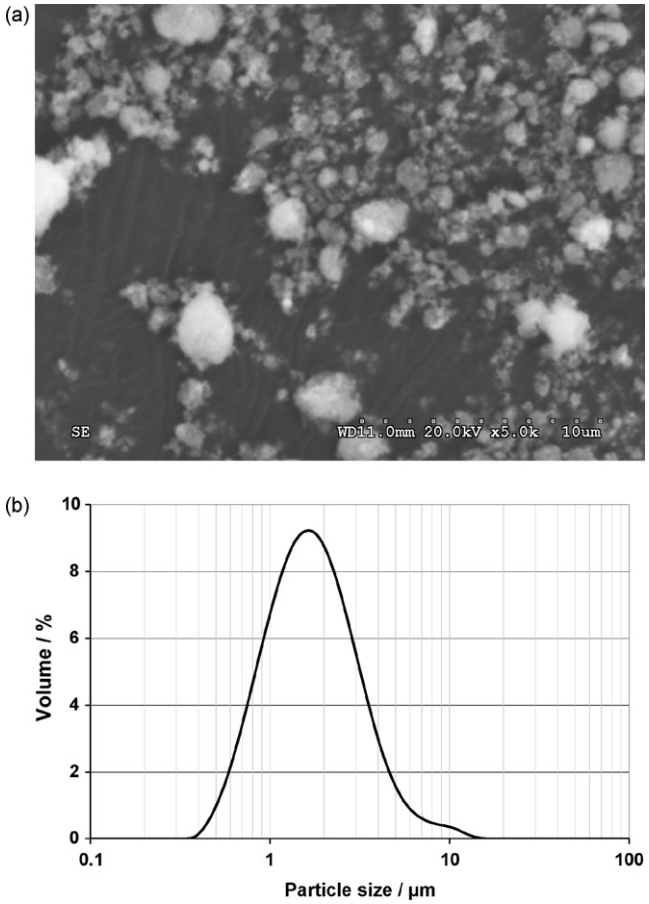

Fig. 1. (a) SEM image and (b) histogram showing the particle size distribution for the YSZ powder used for SPS of the electrolyte.

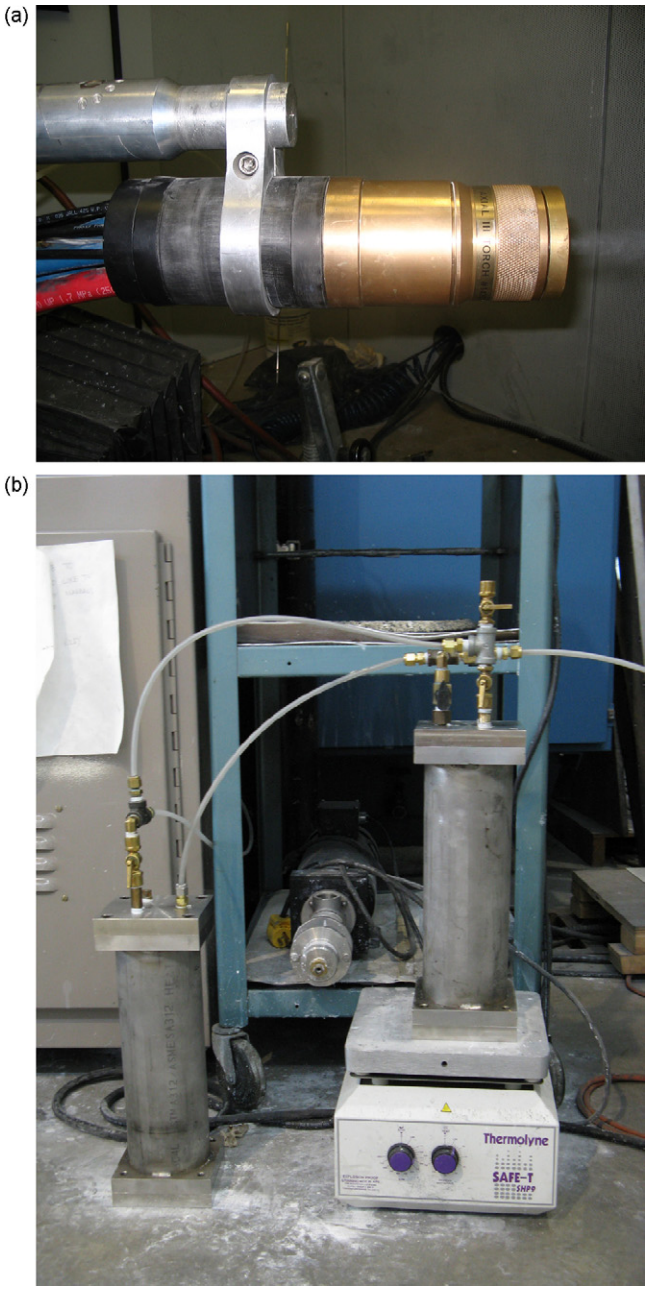

Fig. 2. (a) Mettech Axial III plasma spray torch and (b) pressure vessel based suspension delivery system.

media grade designation refers to the smallest diameter particle in microns that can be captured by the filter material.

Plasma sprayed composite LSM/YSZ cathode layers were first deposited on the steel substrates, followed by the suspension sprayed electrolyte layer. Finally, for the cells that were electrochemically tested, a 1 cm diameter NiO/YSZ anode layer was deposited through a mask in the centre of the electrolyte layer.

The initial electrolyte spraying runs varied one parameter (either preheat temperature, number of passes, or standoff distance) to systematically study the effect of each parameter on the electrolyte permeability, deposition efficiency (thickness), and microstructures.

The plasma spraying parameters used for deposition of each layer are shown in Table 1. Each layer was deposited during a separate spray run of approximately 1–4 min in duration, with no post-deposition heat treatments.

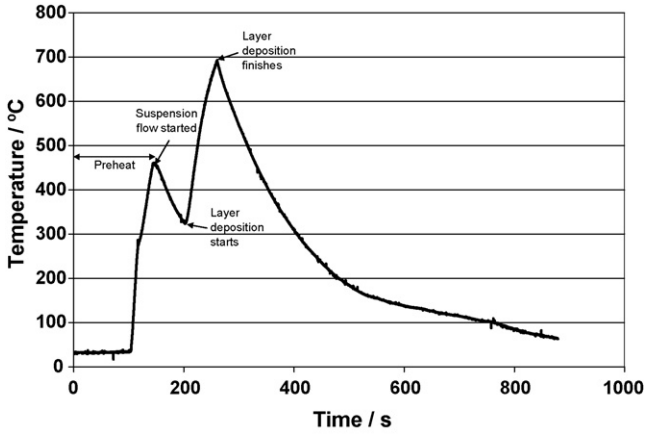

Fig. 3. Temperature measurements during spraying.

2.3. Characterization of plasma sprayed fuel cell layers

The surface roughness of the uncoated and coated samples was measured using surface profilometry (Form Talysurf Series 2, Taylor Hobson Ltd., Leicester, UK). The form analysis software was used to correct for any deviation from horizontal in the substrate-coating pair by using a least squares arc geometric reference. Average roughness values were then calculated.

Helium permeation measurements were performed using an in-house designed fixture in order to measure the gas permeability of the substrates and each deposited layer. The supply of helium gas was regulated at a pressure of 3.5 kPa by a pressure controller (Alicat Scientific, model PCD-5PSIG-D, Tucson, AZ, USA). The flow through the sample was then measured at the outlet of the fixture by a mass flow meter (Alicat Scientific, model M-0.5SCCM-D_H2, Tucson, AZ, USA).

The flow rate through the sample can be related to the layer permeability using Darcy's law (Eq. (1)):

$$Q = \frac{-\kappa A}{\mu}\frac{(P_b - P_a)}{L} \quad (1)$$

where Q is the flow rate ($m^3\ s^{-1}$), κ is the permeability (m^2), A is the cross-sectional area to flow (m^2), $(P_b - P_a)$ is the pressure drop (Pa), μ is the dynamic viscosity (Pa s), and L is the length over which the pressure drop takes place.

For our testing setup, a relative permeability can be calculated by assuming that the cross-sectional area, pressure drop, and dynamic viscosity are constant for each coating tested. Thus a relative permeability (κ) can be calculated by multiplying the measured flow rate (Q) and the electrolyte layer thickness (L). The absolute coating permeability was not directly determined because the substrates were also porous, but since the substrate and cathode thicknesses were the same for different electrolytes tested, a qualitative comparison between conditions was possible.

Polished cross-sections of the deposited layers were examined in a Hitachi S-3000N scanning electron microscope (SEM) (Hitachi High Technologies America, Pleasanton, CA, USA). Samples were cut using a low speed diamond saw, mounted in epoxy, and then polished using diamond polishing suspensions. The polished samples were gold coated to provide sufficient sample conductivity for SEM imaging. The electrolyte layer thickness was measured directly from SEM images.

Electrochemical testing was performed using a custom electrochemical test stand and a Solartron 1480 Multistat (Solartron Analytical, Farnborough, UK). Testing was performed at 650, 700, and 750 °C, and used a humidified (3% H_2O), 20%/80% H_2/N_2 mix-

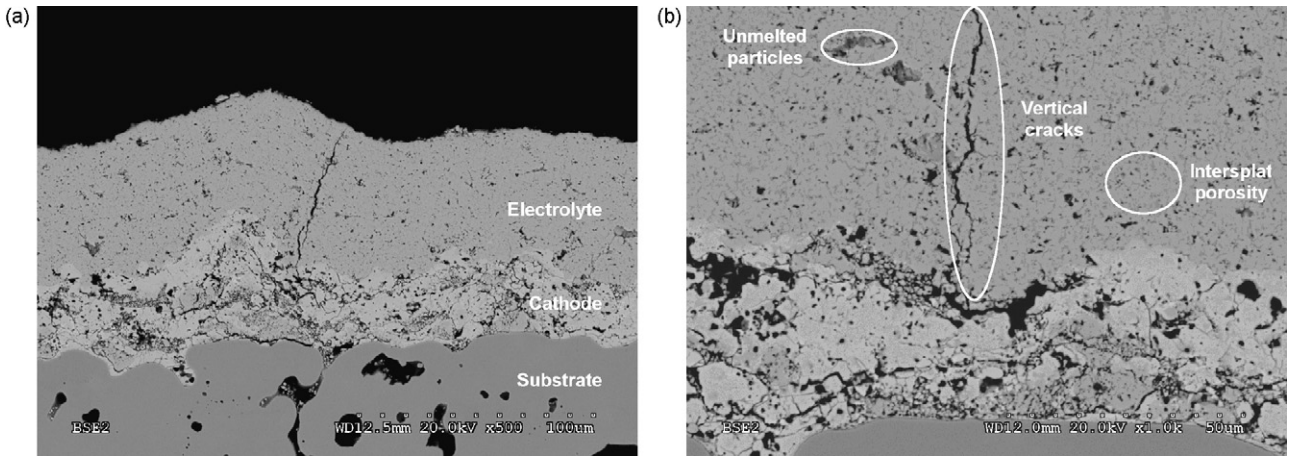

Fig. 4. (a) SEM image of the polished cross-section of a half cell after spraying at the standard conditions (50 deposition passes, 325 °C preheat temperature, 80 mm standoff distance). (b) Defect types seen in suspension plasma sprayed electrolyte layers. The top half of the image is the electrolyte layer, the bottom half is cathode, and the thin strip at bottom centre is the substrate.

ture as the fuel and air as the oxidant. Fuel and air flow rates were set at 200 sccm.

3. Results and discussion

3.1. Initial electrolyte spraying studies

Fig. 4a shows the microstructure of the control sample, which was sprayed at the conditions designated as "standard"—50 deposition passes, 325 °C preheat temperature, 80 mm standoff distance. Electrolyte layers sprayed at these conditions were continuous and mostly dense. Three main defect types were seen in the electrolyte layers: vertical cracking, medium sized defects, and small pores (Fig. 4b). The vertical cracking was likely caused by thermally induced residual stresses produced during spraying. The medium sized defects could be caused by unmelted particles present within the deposited layer, leading to the introduction of porosity around the unmelted particle. Finally, small pores present are likely intersplat porosity.

The effect of number of deposition passes, preheat temperature, and standoff distance on the electrolyte permeation rate and thickness values as well as the cell microstructures are shown in Figs. 5–11. As the number of deposition passes increases, the electrolyte thickness increases and permeation decreases (Fig. 5). However, the permeability of the coatings increases with increasing coating thickness (Fig. 6), suggesting that the porosity of subsequently deposited coating layers may be higher than the porosity of the initial layers in the coatings, possibly due to different rates of solidification. Although the permeability calculated and shown in Fig. 6 corresponds to a combined value for the substrate–cathode–electrolyte system, the permeation through the substrate and cathode have been previously found to be substantially higher than that of the substrate–cathode–electrolyte combination [21], so the total permeability is likely dominated by the properties of the electrolyte.

Fig. 7a and b shows the microstructure of the 25 pass and 100 pass electrolyte layer, respectively. Compared to the standard microstructure (Fig. 4a), the 25 pass electrolyte looks more porous, and it appears that the thinner layer had difficultly bridging over the topography of the cathode surface in places. The thicker electrolyte looks reasonably dense and well adhered to the cathode, but such a thick electrolyte will lead to very high resistive losses during fuel cell operation.

Substrate preheat temperature seemed to have little effect on deposition efficiency, but it appeared that too low of a preheat temperature (20 °C) significantly increased the electrolyte permeation, as seen in both permeation measurements (Fig. 8) and in microstructural examination (Fig. 9), where the unpreheated electrolyte layer (Fig. 9a) looks significantly more porous than the standard microstructure (Fig. 4a). Samples with higher preheat

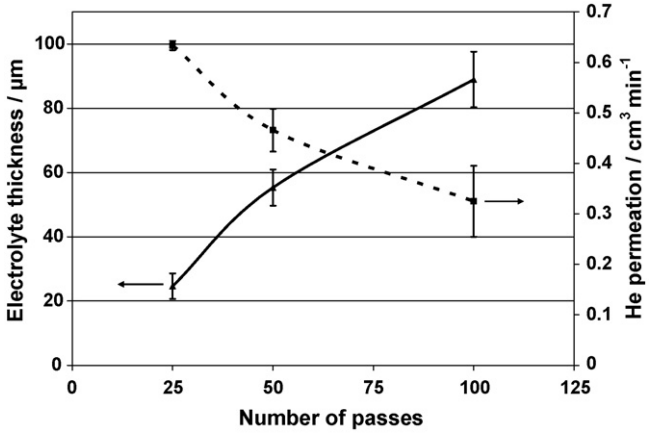

Fig. 5. Effect of number of deposition passes on electrolyte thickness and permeation at 3.5 kPa.

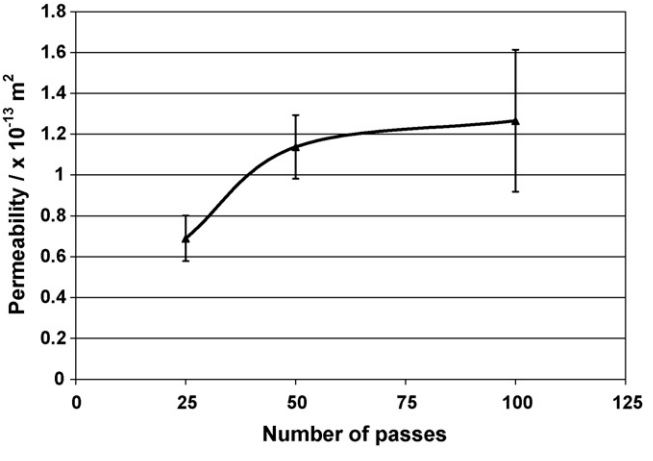

Fig. 6. Effect of number of deposition passes on the permeability of electrolyte coatings on porous metal + cathode substrates.

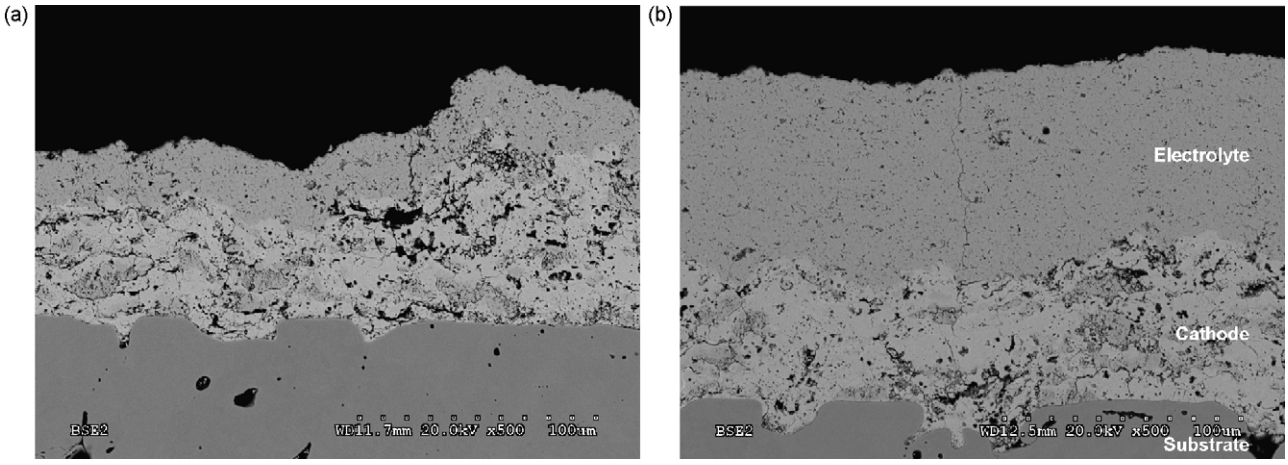

Fig. 7. SEM image of the polished cross-section of the cathode–electrolyte half cell after (a) 25 and (b) 100 electrolyte deposition passes. The labels in (b) also apply to the same layers in (a).

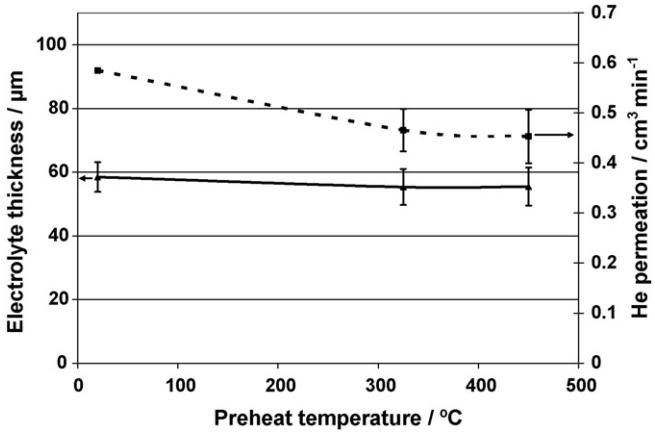

Fig. 8. Effect of preheat temperature on electrolyte thickness and permeation at 3.5 kPa.

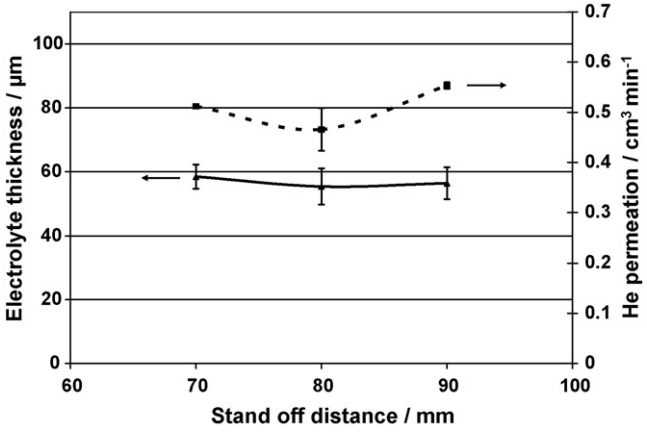

Fig. 10. Effect of standoff distance on electrolyte thickness and permeation at 3.5 kPa.

temperatures (325 or 450 °C) had very similar layer thicknesses, permeations, and microstructures.

Standoff distance seemed to have no effect on the deposition efficiency for the conditions examined in this study as seen in Fig. 10, and the layer microstructures looked fairly similar as well (Fig. 11). The permeation rate of the samples at a standoff distance of 90 mm was significantly higher than those at lower standoff distance, and it appeared that an 80 mm standoff produced coatings with the lowest permeation rate among the standoff distances studied here. The permeabilities of the electrolyte coatings on the substrates as a function of preheat temperature and of standoff distance were also found to follow the same trends as the permeations.

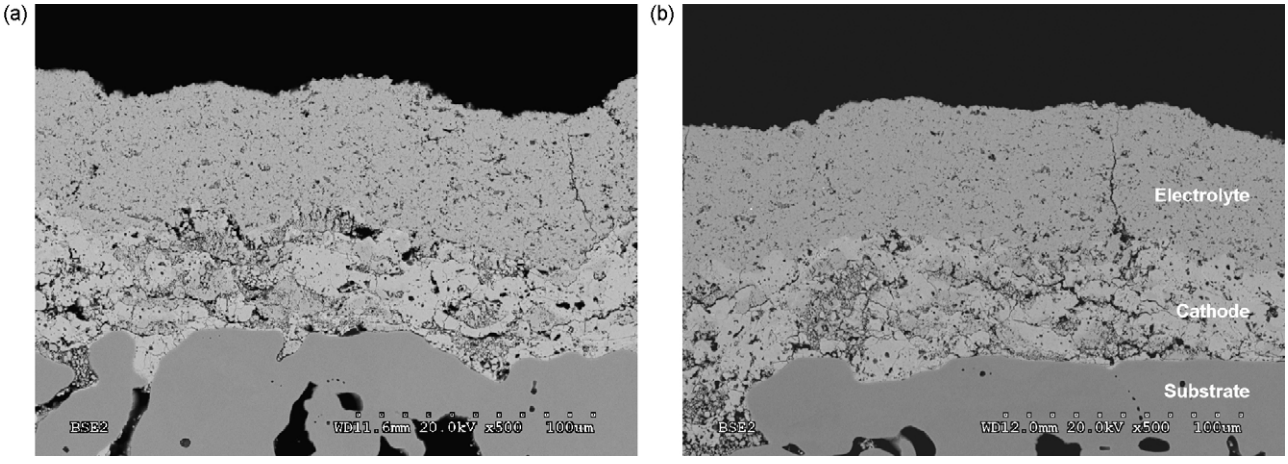

Fig. 9. SEM image of the polished cross-section of half cells with (a) no preheat, and (b) 450 °C preheat. The labels in (b) also apply to the same layers in (a).

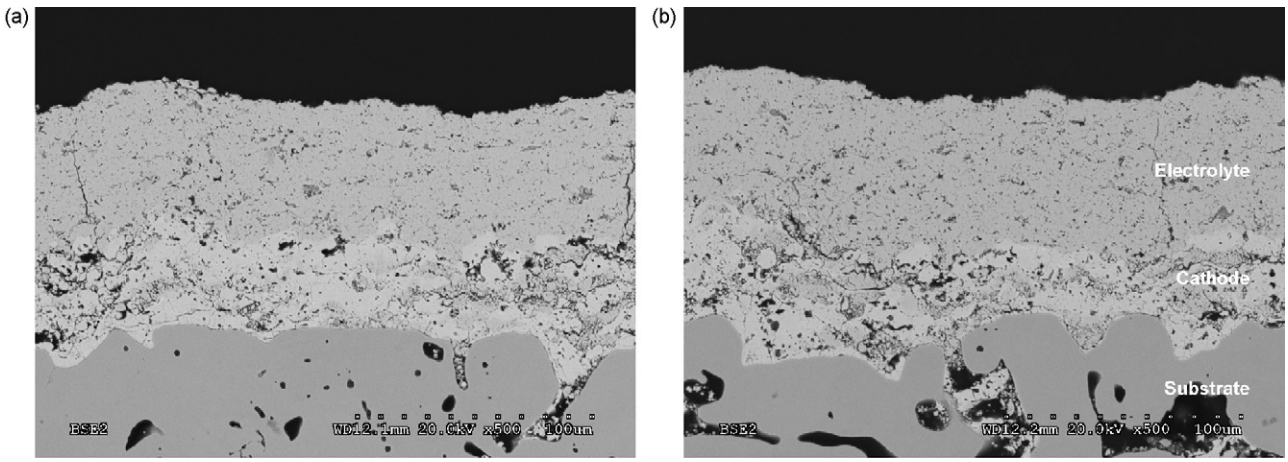

Fig. 11. SEM image of the polished cross-sections of half cells produced at a standoff distance of (a) 70 mm and (b) 90 mm. The labels in (b) also apply to the same layers in (a).

3.2. Substrate characterization

The porosities of both substrate types were calculated from measurements of the weight and dimensions of each substrate. The ratio of this calculated value and the density of a fully dense sample of 430 stainless steel [22] gives the porosity values shown in Table 2.

Table 2
Substrate porosity values.

Substrate	% Porosity
Media grade 2	25.4
Media grade 5	28.1

SEM images of the polished cross-sections of the two substrate types are shown in Fig. 12a and b. Both the amount of porosity

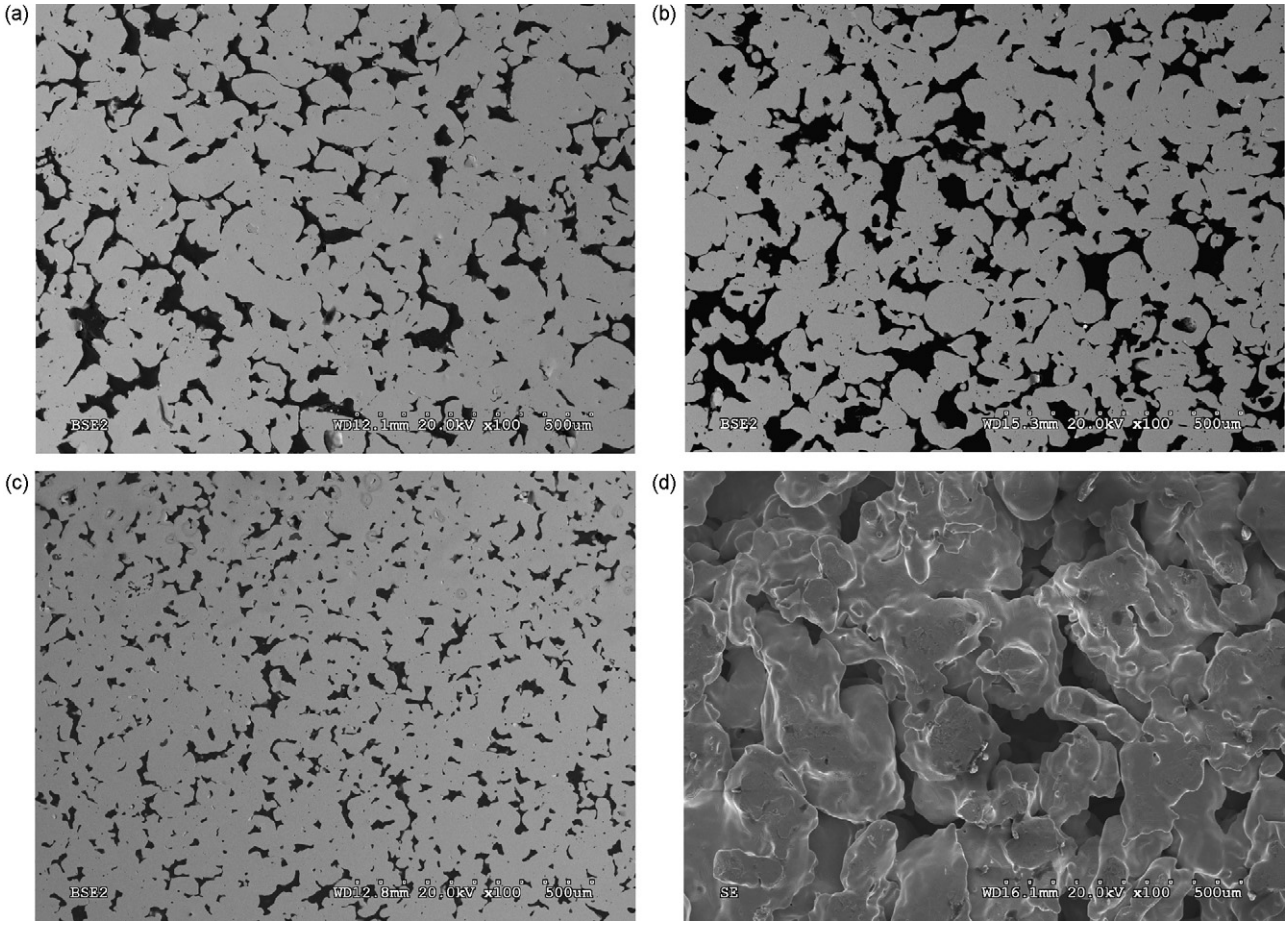

Fig. 12. SEM image of the polished cross-section of (a) the MG 2 substrate, (b) the MG 5 substrate, and (c) the MG 0.5 substrate, and (d) SEM image of the surface of the MG 40 substrate.

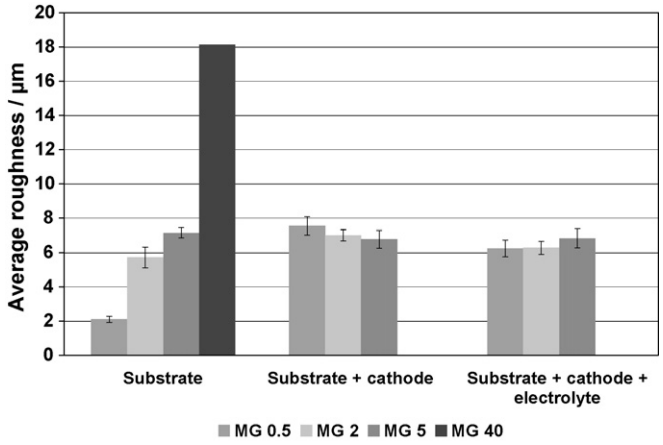

Fig. 13. Summary of surface profilometry results.

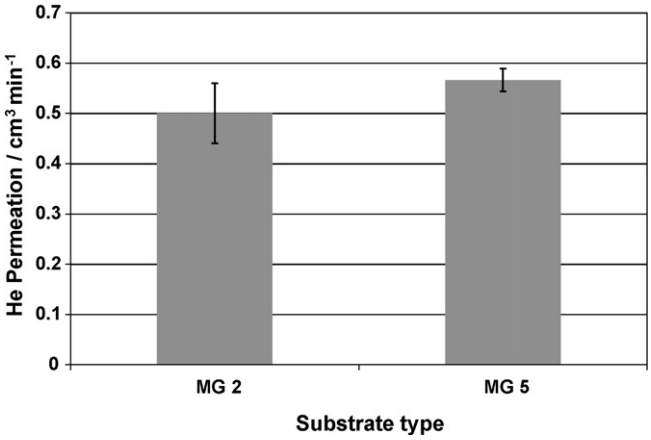

Fig. 14. Summary of permeation testing results at 3.5 kPa of cathode–electrolyte half cells on metal supports.

and the average pore size increase as the substrate media grade increases.

In order for these porous media to perform as SOFC mechanical supports, a balance must be struck between high porosity and large pores that enhance gas diffusion across the support and low porosity and small pores that allow splats to more effectively "bridge" over surface pores to produce continuous coatings. The two media grades 2 and 5 were chosen, as they appear to have a good compromise of porosity (25–30%) and pore size (1–50 μm). Fig. 12c and d shows the microstructures of a substrate with too-low porosity (MG 0.5) and with too-large pores (MG 40) for comparison purposes.

3.3. Surface profilometry

Surface roughness measurements for the MG 2 and 5 substrates are summarized in Fig. 13. Additional measurements for samples with smaller pores (MG 0.5) and larger pores (MG 40) are also shown for comparison purposes. For uncoated substrates, the surface roughness increases with the media grade; however, once a cathode coating is deposited on the porous metal substrates, there is no measurable difference in average cathode surface roughness regardless of which substrate is used for the three lowest media grades studied. Electrolyte surface roughness was also very similar regardless of which substrate was used. Continuous coatings were unable to be deposited on MG 40 substrates due to the large surface pores present.

3.4. Helium permeation testing

Helium permeation tests compared the permeation rate of cathode–electrolyte half cells sprayed on MG 5 substrates to those sprayed on MG 2 substrates. As can be seen in Fig. 14, coatings on MG 5 substrates had slightly higher permeation rates than those sprayed on MG 2 substrates. This is likely due to the larger surface pores present in the MG 5 substrates. These large pores are difficult for the cathode layer to bridge, resulting in a higher probability of discontinuities within the layers and thus higher permeation rates.

3.5. Fuel cell microstructure

The overall microstructures of the full cells on the MG 2 and 5 stainless steel substrates are shown in Fig. 15. The cathode appeared to be well adhered to the porous substrate and was for the most part able to bridge over substrate surface pores. However, there were a few areas where the substrate surface pores were very large, making it difficult for the cathode layer to bridge over the pores (Fig. 16a). This phenomenon produced areas of localized electrolyte thinning, and may indicate that the use of a substrate with smaller surface pores may improve layer continuity. Fig. 16b shows an SEM image of a coating on a MG 2 substrate, showing a region of connected porosity within the electrolyte caused by a cathode irregularity. These cathode irregularities are likely caused by clumping within the feedstock cathode powders.

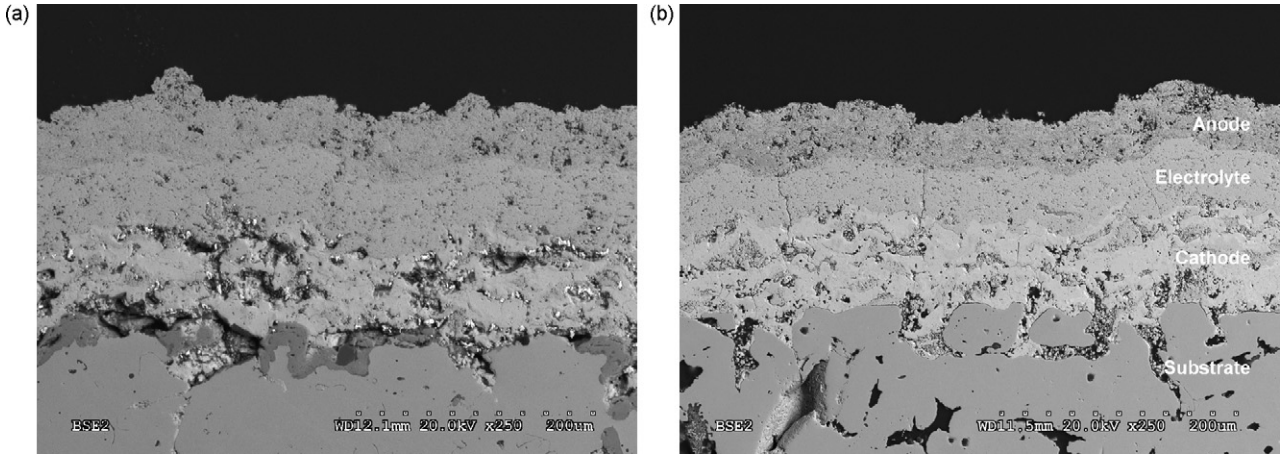

Fig. 15. SEM image of a tested full cell on (a) a MG 2 substrate and (b) a MG 5 substrate. The labels in (b) also apply to the same layers in (a).

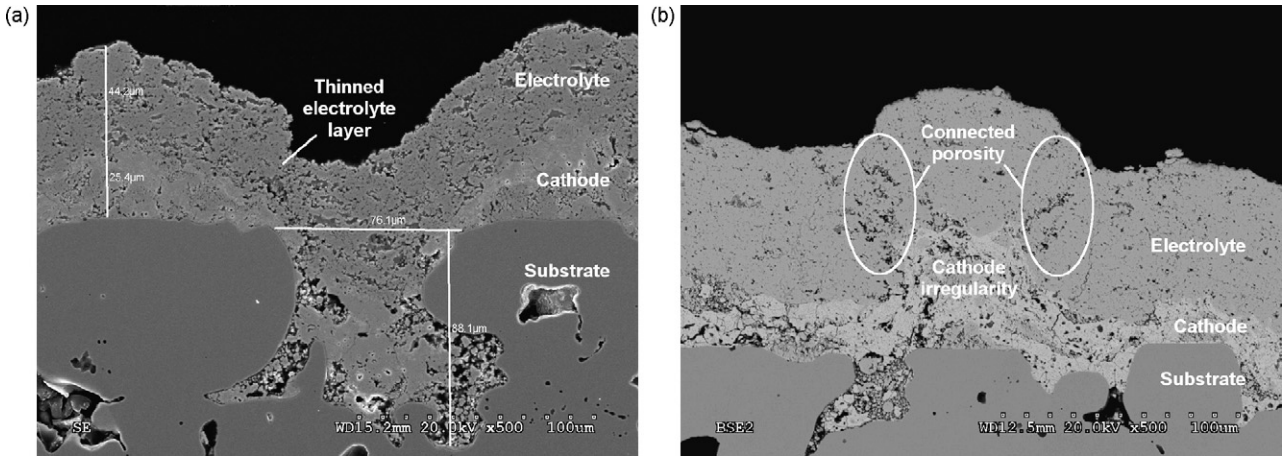

Fig. 16. SEM image of a cathode–electrolyte half cell (a) on a MG 5 substrate, showing large surface pore and the resulting discontinuity in the cathode and electrolyte layers and (b) on a MG 2 substrate, showing connected porosity within the electrolyte caused by cathode irregularity.

Table 3
Summary of layer deposition rates.

Substrate	Layer	Thickness of deposited layer (μm)	Number of spraying b passes	Duration of spray run (min)	Deposition rate (μm min^{-1})
MG 5	Cathode	57.80	40	1.84	31.4
	Electrolyte	46.79	50	2.30	20.3
	Anode	42.98	80	3.69	11.6
MG 2	Cathode	63.09	40	1.84	34.3
	Electrolyte	59.85	50	2.30	26.0
	Anode	41.00	80	3.69	11.1

3.6. Deposition rates

Coating thicknesses were measured from the cross-sectional SEM images. From the thicknesses, deposition rates for each layer were calculated. These results are summarized in Table 3. Layer deposition rates are very fast compared to vapour phase deposition techniques such as PVD or CVD. It is also worth noting that the laboratory-scale rotating turntable available for mounting the substrates resulted in the samples spending only 3% of the total deposition time in front of the plasma torch. However, the plasma spray process can be readily scaled up to large two-dimensional flat surfaces. In those circumstances, the coating rate and deposition efficiency would be further improved by a factor of ~34.

3.7. Electrochemical testing

Fuel cells on MG 2 and 5 stainless steel substrates were electrochemically tested to determine the gas tightness and electrolyte resistance and the electrode activity. Polarization curves for the electrochemical tests are shown in Fig. 17. Tests were performed at 650, 700, and 750 °C in a 3% humidified 20%/80% H_2/N_2 mixture at the anode with air at the cathode. Open circuit voltage and peak power density values are summarized in Table 4, along with the theoretical values of open circuit voltage for the gas mixtures and temperatures used. Cells on MG 2 substrates had similar open circuit voltages to MG 5 supported cells, but had much higher power density values, with larger kinetic losses appearing to account for much of the difference in power density, as seen from the polarization curves at low current densities in Fig. 17. It is also worth noting

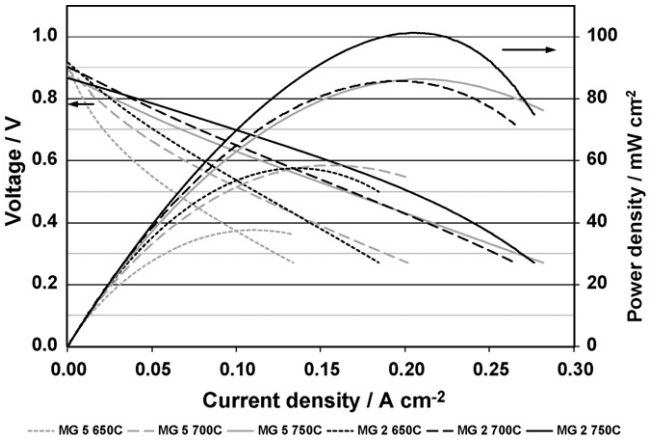

Fig. 17. Polarization and power density curves of a metal-supported plasma sprayed SOFC.

Table 4
Summary of polarization testing results.

Substrate type	Temperature (°C)	Open circuit voltage (V)	Peak power density (W cm^{-2})	Theoretical open circuit voltage (V)
MG 5	650	0.913	0.038	1.06
	700	0.901	0.059	1.05
	750	0.874	0.086	1.04
MG 2	650	0.916	0.058	1.06
	700	0.902	0.086	1.05
	750	0.866	0.101	1.04

that significant mass transport losses appear in the cells tested at 750 °C at a current density of approximately 20 mA cm^{-2}, and at approximately 25 mA cm^{-2} in the cells tested at 700 °C. These differences may be due in part to the limited and non-uniform porosity of the metallic substrates used, as seen, for example, in Figs. 7a and 15a.

However, although operating plasma sprayed metal-supported fuel cells have been produced, significant optimization work is required to increase both the open circuit voltage and the power density. The elimination of large cathode agglomerate particles from the coatings and use of substrates with higher overall porosities and smaller surface pore sizes can both contribute towards the elimination of connected electrolyte porosity, while maintaining sufficient mass transport to the electrode reaction sites.

4. Conclusion

A metal-supported SOFC was successfully fabricated using atmospheric plasma spray manufacturing methods. Plasma sprayed composite cathodes, aqueous suspension plasma sprayed electrolytes, and plasma sprayed composite anodes were deposited in succession on a porous steel substrate. Highly energetic suspension spraying conditions were chosen to ensure that electrolyte materials were fully melted (or nearly fully melted). A selected parameter study of electrolyte spraying conditions found more optimized values for the number of deposition passes, preheat temperature, and standoff distance in order to obtain a good tradeoff between electrolyte permeability, deposition efficiency, and performance. Three main defect types were seen in suspension plasma sprayed electrolyte layers: vertical cracking caused by thermal stresses built up during coating deposition, pores or defects caused by unmelted particles within the coating, and small intersplat pores.

Two types of stainless steel substrates with different levels of porosity and pore size were also examined and the surface roughness, permeation rate, layer microstructure, and electrochemical performance of fuel cells deposited on each substrate type were characterized. Surface roughness values were higher for uncoated substrates with larger MG numbers, but once a cathode layer was deposited, there was no significant difference in roughness values. Samples on MG 5 substrates had larger permeation rates than samples on MG 2 substrates, possibly due to the inability of splats to bridge over the large surface pores present in the MG 5 substrates. Cross-sectional SEM showed that for the most part, layers appear to be well adhered and continuous. On MG 5 samples, there were a few areas where large substrate surface pores resulted in localized thinning of electrolyte layers, and on both substrate types, occasional cathode irregularities occurred that caused connected porosity within the electrolyte layers. Composite cathode and anode layers appeared to be well mixed and to contain some porosity. Electrolyte layers contained a few small, mostly unconnected pores. Polarization testing showed that cells produced on stainless steel MG 2 and 5 substrates had similar open circuit voltage values, but the fuel cells deposited on MG 2 substrates had a significantly higher power density.

Future work on this project will involve optimization of spraying parameters in order to obtain higher surface area and porosity in electrode layer microstructures and to further increase electrolyte gas tightness. The properties of electrolyte feedstock suspensions will also be characterized in order to improve the suspension feedability and dispersion and the resulting electrolyte layer microstructures.

Acknowledgements

The authors gratefully acknowledge financial support from the Natural Sciences and Engineering Research Council of Canada, Northwest Mettech Corporation, and the BC Innovation Council, as well as the assistance of Bradley White, Lars Rose and Dr. Michael Poon with plasma spraying.

References

[1] R. Henne, Journal of Thermal Spray Technology 16 (3) (2007) 381–403.
[2] E. Tang, F. Martell, R. Brulé, K. Marcotte, B. Borglum, in: S.C. Singhal, M. Dokiya (Eds.), SOFC VIII Proceedings, PV2003-07, Paris, France, April 27–May 2, 2003, The Electrochemical Society, 2003, pp. 935–943.
[3] Z.G. Yang, International Materials Reviews 53 (1) (2008) 39–54.
[4] X. Zhang, C. Deces-Petit, S. Yick, M. Robertson, O. Kesler, R. Maric, D. Ghosh, Journal of Power Sources 162 (1) (2006) 480–485.
[5] R. Hui, Z. Wang, O. Kesler, L. Rose, J. Jankovic, S. Yick, R. Maric, D. Ghosh, Journal of Power Sources 170 (2) (2007) 308–323.
[6] C. Zhang, H.L. Liano, W.Y. Li, G. Zhang, C. Coddet, C.J. Li, C.X. Li, X.J. Ning, Journal of Thermal Spray Technology 15 (4) (2006) 598–803.
[7] P. Fauchais, Journal of Physics D: Applied Science 37 (2004) R86.
[8] T. Franco, Z. HoshiarDin, P. Szabo, M. Lang, G. Schiller, Journal of Fuel Cell Science and Technology 4 (4) (2007) 406–412.
[9] M. Lang, R. Henne, S. Schaper, G. Schiller, Journal of Thermal Spray Technology 10 (4) (2001) 618–625.
[10] M. Lang, T. Franco, R. Henne, P Metzger, G. Schiller, S. Ziehm, in: S.C. Singhal, M. Dokiya (Eds.), SOFC VIII, PV2003-07, The Electrochemical Society Proceedings Series, Pennington, NJ, 2003, p. 1059.
[11] R. Zheng, X.M. Zhou, S.R. Wang, T.L. Wen, C.X. Ding, Journal of Power Sources 140 (2005) 217.
[12] X.Q. Ma, H. Zhang, J. Dai, J. Roth, R. Hui, T.D. Xiao, D.E. Reisner, Journal of Thermal Spray Technology 14 (1) (2005) 61.
[13] J. Oberste Berghaus, S. Bouaricha, J.G. Legoux, C. Moreau, in: E.F. Lugscheider (Ed.), International Thermal Spray Conference (ITSC) 2005 Proceedings, Basel, Switzerland, May 2–4, 2005, pp. 1434–1440.
[14] J. Oberste Berghaus, S. Bouaricha, J.G. Legoux, C. Moreau, T. Chráska, in: E.F. Lugscheider (Ed.), International Thermal Spray Conference (ITSC) 2005 Proceedings, Basel, Switzerland, May 2–4, 2005, pp. 512–518.
[15] C. Delbos, J. Fazilleau, J.F. Coudert, P. Fauchais, L. Bianchi, K. Wittmann-Teneze, in: B.R. Marple, C. Moreau (Eds.), Thermal Spray 2003: Advancing the Science and Applying the Technology Proceedings, Orlando, FL, USA, May 5–8, 2003, ASM International, 2003, pp. 661–669.
[16] V. Rat, C. Delbos, C. Bonhomme, J. Fazilleau, J.F. Coudert, P. Fauchais, High Temperature Material Processes 8 (1) (2004) 95–117.
[17] M. Bonneau, F. Gitzhofer, M. Boulos, International Thermal Spray Conference (ITSC) 2000 Proceedings, Montreal, Quebec, Canada, May 8–11, 2000, pp. 929–934.
[18] J. Oberste Berghaus, J.G. Legoux, C. Moreau, R. Hui, C. Decès-Petit, W. Qu, S. Yick, Z. Wang, R. Maric, D. Ghosh, International Thermal Spray Conference (ITSC) 2008 Proceedings, Maastricht, The Netherlands, May 1–4, 2008, pp. 183–189.
[19] R. Rampon, O. Marchand, C. Filiatre, G. Bertrand, Surface & Coatings Technology 202 (18) (2008) 4337–4342.
[20] B.D. White, O. Kesler, L. Rose, Journal of Power Sources 178 (1) (2008) 334–343.
[21] D. Waldbillig, O. Kesler, Surface and Coatings Technology 203 (2009) 2098–2101.
[22] H.E. Boyer, T.L. Gall (Eds.), Metals Handbook Desk Edition, American Society of Metals, Metals Park, OH, 1985, pp. 1–49.